Dalton Transactions

Accepted Manuscript

ROYAL SOCIETY OF CHEMISTRY

www.rsc.org/dalton

Thermoelectric Properties of Higher Manganese Silicide / Multi-Walled Carbon Nanotubes Composites

D. Y. Nhi Truong[1,2], Holger Kleinke[2], Franck Gascoin[1]

1 Laboratoire CRISMAT UMR 6508 CNRS ENSICAEN, 6 boulevard du Maréchal Juin, 14050 Caen Cedex 04, France

2 Department of Chemistry and Waterloo Institute for Nanotechnology, University of Waterloo, Waterloo, Ontario, Canada N2L 3G1

Corresponding author : Franck Gascoin

franck.gascoin@ensicaen.fr

Abstract

Composites made of Higher Manganese Silicides (HMS) – based compound $MnSi_{1.75}Ge_{0.02}$ and multi-walled carbon nanotubes (MWCNTs) have been prepared by an easy and effective method including mechanical milling under mild conditions and reactive spark plasma sintering. SEM compositional mappings show a homogeneous dispersion of MWCNTs in HMS matrix. Electronic and thermal transport properties were measured from room temperature to 875K. While power factors are virtually unchanged by the addition of MWCNTs, the lattice thermal conductivity is significantly reduced by about 30%. As a consequence, the maximum

figure of merit for the composites with 1 wt.-% MWCNTs is improved by about 20% compared to the MWCNTs free HMS-based sample.

Introduction

Higher Manganese Silicides (HMS) are potential candidates for p-type legs for thermoelectric modules. They consist of two cheap and nontoxic elements, possess high mechanical strength, and are thermally and oxidatively stable from room to moderate temperature (up to 900K). Under the HMS appellation, various compounds exist including Mn_4Si_7, $Mn_{11}Si_{19}$, $Mn_{15}Si_{26}$, and $Mn_{27}Si_{47}$, all crystallizing with the Nowotny chimney-ladder structure type [1-3]. These structures can be described as built up of Mn and Si sublattices, where the Mn atoms form the chimneys in which the Si atoms are arranged as ladders. The tetragonal unit cells of different HMS compounds have similar *a* parameter, and different *c* parameters, depending on the ratio c_{Si}/c_{Mn} of the two sublattices. Recently, a variety of studies has been conducted on tuning the transport properties of polycrystalline HMS to improve their performance for thermoelectric applications [4-6]. However, the efficiency of HMS-based materials still remains at a moderate level as their thermoelectric figure of merit is typically not greater than 0.6 [5]. This is mainly due to their high thermal conductivity compared to conventional materials such as Bi_2Te_3 or PbTe. Interestingly, the dominant contribution of the thermal conductivity of HMS comes from the phononic term that represents approximately 70% of the total value [7]. Therefore, one strategy to improve the thermoelectric performance of HMS consists in reducing their lattice thermal conductivity.

It has been previously reported that the introduction of selected secondary phases within the matrix can increase the phonon scattering at the interfaces e.g; at the grain boundaries. Some

examples of these composites are given as Si nanowires/ Ge [8], single-walled carbon nanotubes/ Si_3N_4 [9], amorphous SiO_2 nanoparticles/ $(Bi_2Te_3)_{0.2}(Sb_2Te_3)_{0.8}$ [10], or graphene/ PbTe [11], where the prior phases are the added secondary phases, and the later ones are the matrix materials. For HMS, several works on different composites have been reported, utilizing secondary materials such as Ag_2Te [7], PbTe [7], $CeSi_2$ [12], SiGe [13] and *in situ* formed [14] and externally processed [15] MnSi. In all these cases with the exception of $CeSi_2$, a reduction of thermal conductivity is observed and attributed to the enhancement of phonon scattering due to increased impurity concentration at the grain boundaries. The sizes and distributions of these secondary phases are considered to affect the transport properties of the host materials. A random distribution of Ag_2Te and PbTe micro grains [7], $CeSi_2$ fine particles [12], and Si-Ge micro dots and strips [13] along the grain boundaries of HMS materials was noticed. From the composites with Ag_2Te and PbTe, A. J. Zhou *et al*. [7] have firstly proposed that a fine dispersion is necessary to enhance the thermoelectric performance of HMS-based composites. Furthermore, W. Luo *et al*. [14] prepared *p*-type HMS with *in situ* formed nano-sized and evenly distributed MnSi, and reported a huge improvement of more than 50% of the thermoelectric figure of merit up to 0.62 at 800 K compared to that with micro-sized, and unevenly distributed MnSi. Lately, X. Shi *et al*. [15] added a small amount (about 1 at.-%) of externally processed, nanostructured MnSi to $MnSi_{1.75}$, and observed a reduction in both lattice and ambipolar thermal conductivity, but the morphology and distribution of the secondary phase was not clarified in the report.

Since the discovery of MWCNTs more than two decades ago, they have been widely used in many industrial applications such as conductive polymers, electromagnetic interference shielding composites, and electrostatic dissipation. MWCNTs are endowed with exceptional properties including high electrical conductivity (as conductive as copper), and high mechanical

strength (up to 20 times stronger than steel). Moreover, they are light weight, flexible, thermally stable and chemically inert [16]. In this contribution, composites carbon nanotubes (MWCNTs) / HMS-based material are synthesized and their transport properties are studied with the aim of improving thermoelectric properties.

Experimental section

Higher Manganese Silicides (HMS)-based composites are synthesized from the high purity elements purchased from Alfa Aesar as followed: Mn powder, 99.95%, -325 mesh; Si powder, crystalline, 99.9%, -100 mesh; Ge powder, 99.999%, -100 mesh; and multi-walled carbon nanotubes (MWCNTs) powder, 6 to 9 nm in diameter by up to 5 μm long, > 95% (carbon) from Sigma-Aldrich. A simple and effective synthetic process is carried out involving two steps, namely: mechanical milling and spark plasma sintering (SPS). The stoichiometric amounts of the elements, e.g. $MnSi_{1.75}Ge_{0.02}$ + the MWCNTs, are blended via planetary ball milling using vials and balls made of tungsten carbide. Soft conditions are used with a ball-to-powder weight ratio of 3:1, a slow speed of 400 rpm, and a total duration of 20 minutes divided into two periods of rotation in reverse directions. The obtained homogeneous mixtures are directly loaded into graphite die for SPS at 1050°C in 45 minutes using a maximum pressure of 28 MPa.

Quality of the samples is checked at each step of the process by means of X-ray powder diffraction using a Phillips X-Pert Pro Panalytical diffractometer with a $K_{\alpha1}/K_{\alpha2}$ radiation (λ = 1.540598 Å, 1.544426 Å). The microstructure and chemical analysis are studied by an energy dispersive X-ray scanning electron microscope (SEM/EDX) Carl ZEISS SUPRA 55. The density of the materials, d, is determined via the Archimedes' method given as $d/d_{liquid} = m_{air}/(m_{air} - m_{liquid})$, where m_{air} is the weight of the sample in the air, m_{liquid} is the weight of the same piece

completely submerged in the liquid, and d_{liquid} is the density of the liquid. All the samples have densities higher than 93% of the theoretical density, which is satisfactory for subsequent physical property measurements considering the error range of the density determinations.

The sintered pucks are cut into bars of approximate sizes of 10 × 3 × 3 mm^3 and square pieces of 6 × 6 × 1 mm^3 for electrical and thermal property measurements, respectively. The electrical resistivity and Seebeck coefficient are simultaneously measured using a ZEM-3 system (ULVAC-RIKO). The thermal diffusivity, α, is obtained by using a laser flash diffusivity method with a Netzsch's LFA 457 Micro Flash measuring system. The thermal conductivity, κ, is then calculated by $\kappa = \alpha \times C_p \times d$, where C_p is the specific heat capacity calculated via the Dulong-Petit law, formulated as $C_p = 3R/\bar{M}$ with R is the gas constant, and $\bar{M}$ is the average molar mass per atom. It must be noted that all the C_p were measured and they all fall within 10% of the Dulong Petit value, we thus used the C_p of the pure HMS for all the samples, e.g. 0.655 J/g/K.

Results and discussions

The combination of ball milling and spark plasma sintering is used to prepare HMS and composites made of commercial MWCNTs and HMS matrix. A nominal formula of $MnSi_{1.75}Ge_{0.02}$ was chosen as addition of Ge has been reported to improve the thermoelectric properties of HMS. Moreover, a solubility limit of about 1.6% has been determined. Our choice of $MnSi_{1.75}Ge_{0.02}$ (that is 1.1% of Ge on the Si site, well below the solubility limit) is thus based on the reported improvement [17]. The rather gentle ball milling conditions utilized (400 rpm for 20 minutes) are sufficient to reduce the particle sizes of the elemental precursors but also assure their intimate mix. The same technique was previously used to prepare magnesium silicides (Mg_2Si), and it was proven that a short heating process either using microwave radiation [18],

regular resistance furnace [19] or spark plasma sintering [20] was enough to trigger and complete the reaction. Here, the intimately mixed, fine powders of the elemental precursors are directly subjected to a spark plasma sintering cycle, the resulting pucks have measured densities typically of at least 93% of the theoretical one. This process has evident advantages as it is fast and requires fairly low amount of energy, both important parameters when considering the mass production of any materials. Pucks of up to 50 grams each have been prepared, however, in this study, 15 mm diameter pucks were fabricated. In order to also insure the ideal mix of the MWCNTs and the (Mn,Si,Ge) powders, the MWCNTs were introduced in the milling jar and consequently, also subjected to the ball milling step.

The phase constitutions are identified by powder X-ray diffraction of the ground samples after the sintering process, all showing the major phase to be the desired HMS with traces of MnSi and Si. The introduction of carbon nanotubes does not bring any extra peaks on the X-ray powder pattern (See supplementary information). The typical morphologies of MWCNTs/ HMS-based composites are shown in Figure 1 for the sample with 1 wt.-% MWCNTs. Micro pores and cracks are visible, similarly to what was reported by X. Chen *et al*. [21]. Few impurities of elemental Si and MnSi phases are also seen as distinct islands with different sizes ranging up to several microns in HMS matrix. The presence of these two phases is not surprising as it is well known that it is difficult to obtain HMS as single phase, moreover, the presence of MnSi is usually detrimental to the thermoelectric performance as its metallic character contributes to an increased thermal conductivity [22]. Interestingly, it should be mentioned that there is no observation of carbon agglomerations for the samples with 0.1, 0.2, and 0.5 wt.-% MWCNTs, however some carbon clusters become visible for the sample with 1 wt.-% MWCNTs as indicated in the same figure. The elemental mappings of the sample with 1 wt.-% MWCNTs are

presented in Figure 1 (b) for the four constituting elements Mn, Si, Ge, and C. Overall the sample is homogenous and the MWCNTs, even at this high volume concentration, are distributed quite uniformly in the HMS matrix, again with the exception of some minor clusters.

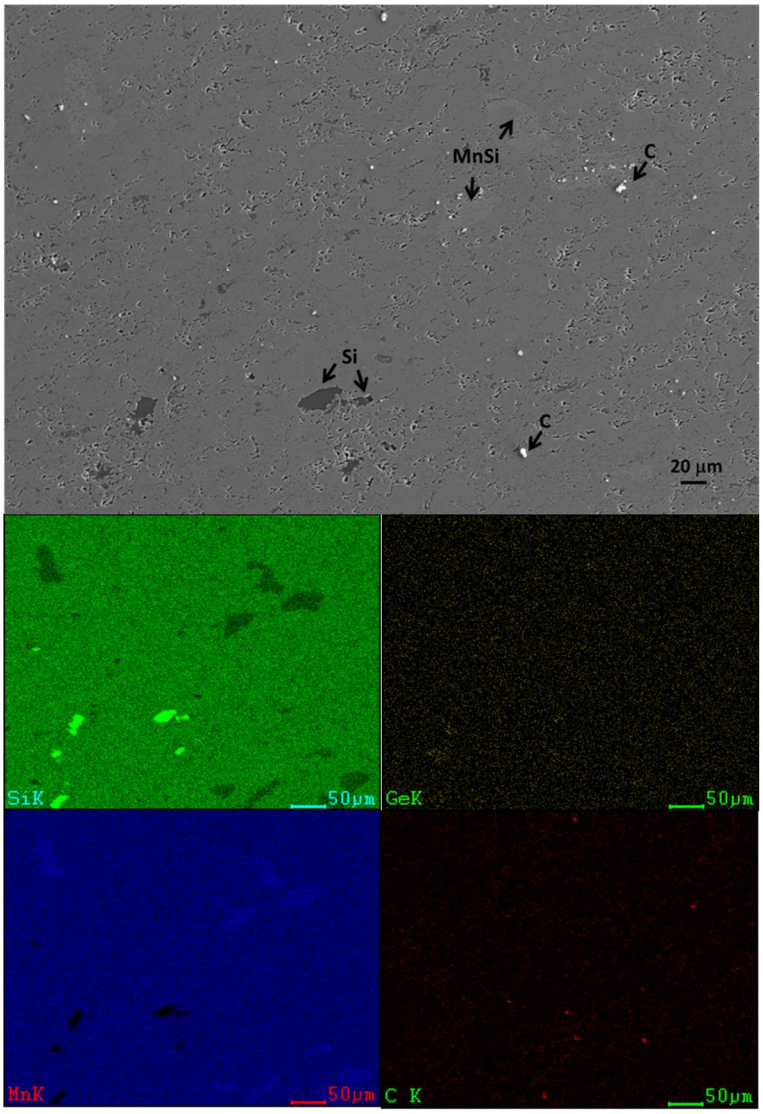

Figure 1 : SEM image (top) and elemental mapping (bottom) of the MWCNTs/ HMS composite with 1 wt.-% MWCNTs

The calculated densities of MWCNTs / HMS-based composites are given in Table 1. The theoretical values, d_C, are also given in comparison, formulated as $1/d_C = W_{CNT}/d_{CNT} +$

W_{HMS}/d_{HMS}, where W_{CNT} and W_{HMS} are the mass fractions of MWCNTs and HMS-based material, respectively, d_{CNT} is the density of MWCNTs given by the manufacturer, and d_{HMS} is the density of $MnSi_{1.75}Ge_{0.02}$ calculated from that of $MnSi_{1.75}$ with the assumption that the addition of a small amount of Ge does not change significantly the unit cell of HMS [23]. All the composites prepared have experimental densities higher than 93% of the theoretical one allowing us to proceed to the physical property measurements. These results might even be underestimated as the SEM observations show very little residual porosity, typically less than 3%. In turn, this underestimation might come from the error inherent to the measurement of the density together with the actual calculation of the theoretical density.

Nominal MWCNTs content (wt.-%)	Theoretical density (g/cm^3)	Experimental density (g/cm^3)	Percentage (%)
0.0	5.22	4.96	95
0.1	5.21	4.93	95
0.2	5.20	4.94	95
0.5	5.18	4.90	95
1.0	5.14	4.79	93

Table 1. Nominal MWCNTs content, theoretical and experimental densities of MWCNTs/ HMS-based composites

Room temperature transport data are given in table 2. They indicate that the carrier concentration is not modified by the addition of MWCNTs, result in good agreement with the quasi constant value of the Seebeck coefficient (estimated 15% and 5% errors are generally accepted for the measurements of carrier concentration and Seebeck coefficient, respectively). However, an increase of electrical resistivity is noticeable with the addition of MWCNTs, concomitant with a slightly decreasing mobility. Since this effect does not seem to come from any sorts of doping that would have also affected the Seebeck coefficient, it can be reasonably postulated that the introduction of MWCNTs within HMS matrix affects the microstructure in a way that disturbs the electron flow because of a greater grain boundary scattering. As the

electrical conductivity of MWCNTs depends on their structure, it is possible that different results might be found depending on the source of MWCNTs used and whether or not they are more conducting than the HMS matrix. However, in this study, only microstructural effects can be evidenced. Evidently, if the addition of MWCNTs degrades the electronic transport, it also degrades the thermal transport as demonstrated by the evolution of the room temperature thermal diffusivity that drops from 1.28 mm^2/s in the MWCNTs free sample to 0.91mm^2/s in the 1 wt. % sample, a rather impressive 30% decrease.

Nominal MWCNTs content (wt.-%)	n_p (10^{21} cm^{-3})	μ_p $cm^{-2}/V/s$	S ($\mu V/K$)	ρ ($m\Omega.cm$)	α (mm^2/s)
0	2.19	1.71	127	1.66	1.28
0.1	2.81	1.33	123	1.65	1.19
0.2	2.27	1.57	119	1.74	1.06
0.5	2.15	1.54	119	1.87	0.95
1.0	3.00	1.05	124	1.96	0.91

Table 2: Room temperature carrier concentration (n_p), mobility (μ_p), Seebeck coefficient (S), electrical resistivity (ρ) and thermal diffusivity (α) of the different samples prepared

The HMS being a promising thermoelectric material for medium range temperature applications (typically below 900K), the transport properties of the prepared samples have been measured up to 850K. Figure 2 shows the evolution of the Seebeck coefficient with temperature. For all the samples, the Seebeck coefficient increase with temperature, however, if there are only slight differences at low temperature, the two samples the richest in MWCNTs have higher Seebeck coefficient than the other samples at high temperature, reaching value above 200 $\mu V/K$ above 700K. In parallel, these two samples have also the highest electrical resistivity (Figure 3) as they both reach values higher than 3.5 $m\Omega.cm$ above 800K, the resulting power factor of all the samples is almost independent of the MWCNTs content since the (slightly) increased Seebeck is compensated by the slightly increased electrical resistivity. An explanation of this behavior that

can be hypothesized is a possible electron filtering effect at the grain boundaries, thus enhancing the Seebeck coefficient, coupled with reduced electrical conductivity due to the increased number of grain boundaries.

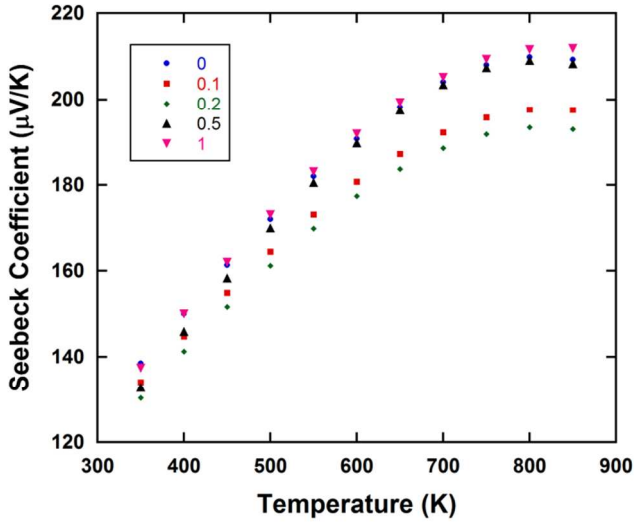

Figure 2 : Temperature dependence of the Seebeck coefficient for the different composites

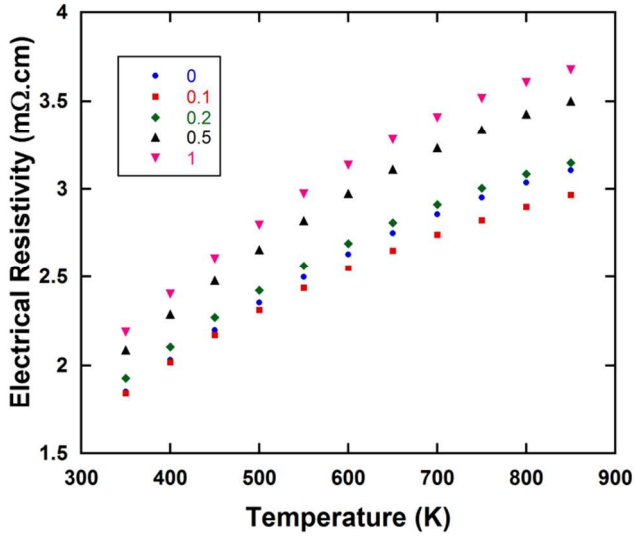

Figure 3 : Temperature dependence of the electrical resistivity for the different composites

What is more striking – and somewhat expected – is the effect of the addition of MWCNTs on the thermal transport properties. The thermal diffusivity of the different composites is shown in Figure 4.

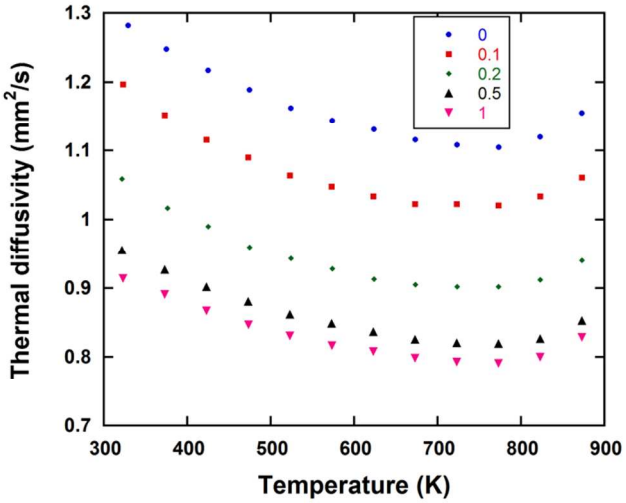

Figure 4 : Temperature dependence of the thermal diffusivity for the different composites

Clearly, it gradually decreases with increasing MWCNTs content. Along the full temperature range, the difference between the MWCNTs free compound and the 1.0 wt.-% MWCNTs composite is about 30%. This notable reduction directly affects the variation of the thermal conductivity as show on Figure 5.

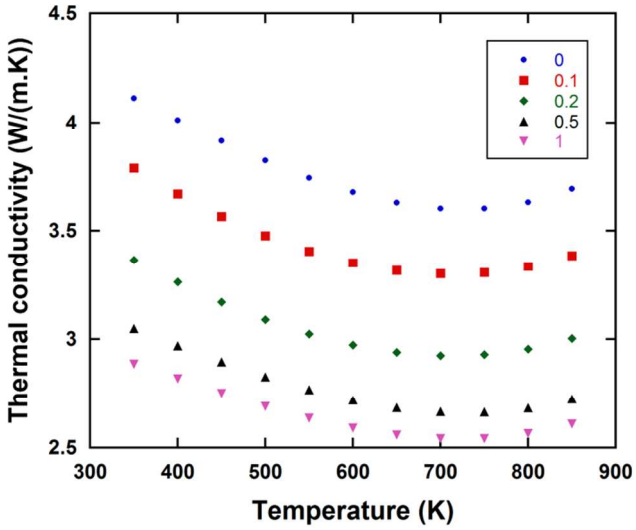

Figure 5 : Temperature dependence of the total thermal conductivity for the different composites

The addition of MWCNTs, indeed, participates in the increase of the phonon scattering, this is also visible on the evolution of the lattice thermal conductivity (Figure 6) that can be extracted from the values of the total thermal conductivity and the electrical resistivity, for the sake of comparison, the electronic component of the thermal conductivity has also been plotted for each compounds on the same figure.

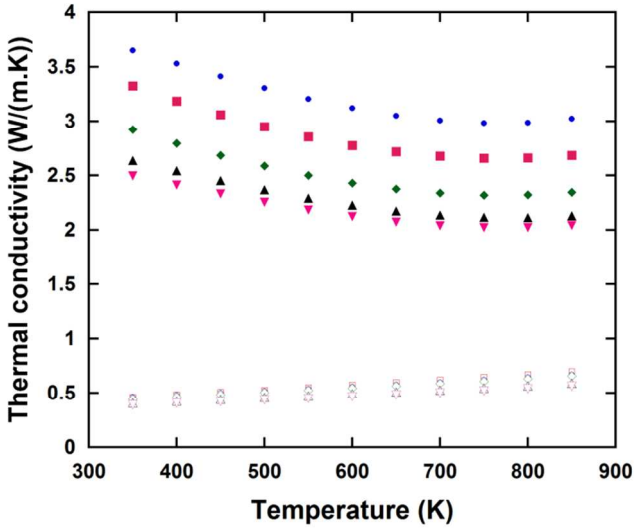

Figure 6 : Temperature dependence of the electronic (empty markers) and phononic component (filled markers) of the thermal conductivity for the different composites (unit for both y axis: W/(m.K))

It thus appears that the electronic component is nearly independent of the MWCNTs content and that the thermal conductivity of the composites (and of HMS in general) is mainly driven by its lattice component, and that even with the addition of MWCNTs, it remains fairly high (above 2 W/(m.K)) but drops dramatically compared to the MWCNTs free sample.

As a consequence of a nearly unchanged power factor, together with a decrease of total thermal conductivity, the thermoelectric figure of merit increases with MWCNTs content. In this study, a zT of 0.4 at 850K is achieved (Figure 7).

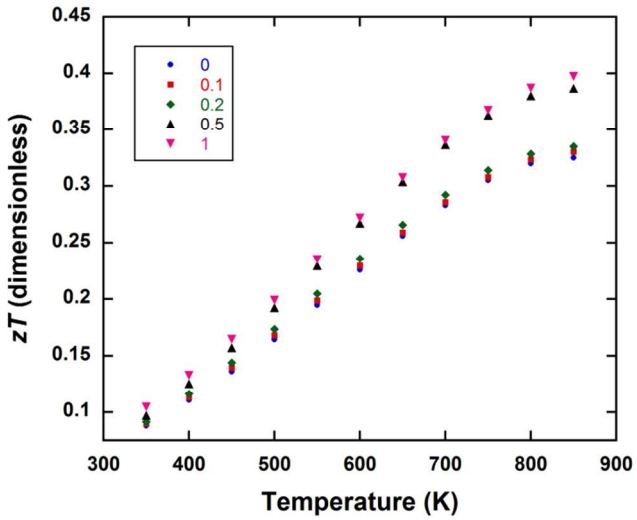

Figure 7 : Temperature dependence of the thermoelectric figure of merit for the different composites

This value is relatively low but the – most likely – detrimental presence of MnSi metallic impurities, usually contributing to an increased thermal conductivity [22], also hinders the thermoelectric properties. Efforts are underway to adjust the parameters of synthesis in order avoid the presence of MnSi and Si impurities.

Conclusion

To summarize, the composites between MWCNTs and HMS-based material have been prepared by an easy and effective method. Indeed, short ball milling time coupled with spark plasma sintering lead to the fast fabrication of sizable samples. Using this simple method, MWCNTs have been evenly dispersed within the HMS-based matrix. The addition of MWCNTs has a huge effect on reducing the thermal diffusivity of the composite material, while the electrical properties are not or much less affected by the introduction of this secondary phase. To the best of our knowledge, this is the first attempt to introduce a carbon-based secondary phase into bulk HMS-based materials. The only other report concerning carbon addition is from Q. R. Hou *et al*. [24] for polycrystalline HMS films prepared by magnetron sputtering, which is beyond the scope of this investigation. The preliminary results show a promising improvement of figure of merit up to 20% with 1 wt.-% MWCNTs. We believe that the performance of these composites can be further enhanced through the optimization of the conditions of synthesis and processing, including adding more than 1wt.-% of MWCNTs. Moreover, considering the numerous sorts of MWCNTs that are commercially available, it is reasonable to assume that depending on the nature of the MWCNTs used in the composites, thermoelectric properties performance could be improved.

Acknowledgement

The authors would like to thank the Region Basse Normandie for the financial support of D.Y. Nhi Truong. The authors are grateful for the technical assistance for the SPS experiments provided by Francois-Xavier Lefevre and Jérome Lecourt. The authors also thank Dr. D. Berthebaud for help concerning the X-ray analysis. The work was furthermore partly supported by the Natural Sciences and Engineering Research Council of Canada in form of a Discovery Grant.

References

1. H. Nowotny, *The Chemistry of Extended Defects in Non-Metallic Solids*, edited by L. Eyring and M. O'Keeffe, North Holland, Amsterdam, 223 (1970)
2. J. M. Higgins, A. L. Schmitt, L. A. Guzei, and S. Jin, *J. Am. Chem. Soc.* **130**, 16086 (2008)
3. Y. Miyazaki, D. Igarashi, K. Hayashi, T. Kajitani, and K. Yubuta, *Phys. Rev. B* **78**, 214104 (2008)
4. I. Aoyama, H. Kaibe, L. Rauscher, T. Kanda, M. Mukoujima, S. Sano, and T. Tsuji, *Jpn. J. Appl. Phys.* **44**, 4275 (2005)
5. W. Luo, H. Li, F. Fu, W. Hao, and X. Tang, *J. Electron. Mater.* **40**, 1233 (2011)
6. P. Norouzzadeh, Z. Zamanipour, J. S. Krasinski, and D. Vashaee, *J. Appl. Phys.* **112**, 124308 (2012)
7. A. J. Zhou, X. B. Zhao, T. J. Zhu, Y. Q. Cao, C. Stiewe, R. Hassdorf, and E. Mueller, *J. Electron. Mater.* **38**, 1072 (2009)
8. R. Yang, G. Chen, and M. S. Dresselhaus , *Phys. Rev. B* **72**, 125418 (2005)
9. E. L. Corral, H. Wang, J. Garay, Z. Munir, and E. V. Barrera, *J. Eur. Ceram. Soc.* **31**, 391 (2011)
10. Y. C. Dou, X. Y. Qin, D. Li, L. L. Li, T. H. Zou, and Q. Q. Wang, *J. Appl. Phys.* **114**, 044906 (2013)
11. J. Dong, W. Liu, H. Li, X. Su, X. Tang, and C. Uher, *J. Mater. Chem. A* **1**, 12503 (2013)

12. A. J. Zhou, T. J. Zhu, H. L. Ni, Q. Zhang, and X. B. Zhao, *J. Alloys Compd*. **455**, 255 (2008)

13. A. J. Zhou, X. B. Zhao, T. J. Zhu, S. H. Yang, T. Dasgupta, C. Stiewe, R. Hassdorf, and E. Mueller, *Mater*. *Chem*. *Phys*. **124**, 1001 (2010)

14. W. Luo, H. Li, Y. Yan, Z. Lin, X. Tang, Q. Zhang, and C. Uher, *Intermet.* **19**, 404 (2011)

15. X. Shi, Z. Zamanipour, K. F. Ede, J. S. Krasinski, and D. Vashaee, *Enhancement of Thermoelectric Efficiency of* $MnSi_{1.75}$ *with the Addition of Externally Processed Nanostructured MnSi*, Green Technologies Conference, 2012 IEEE

16. M. F. L. De Volder, S. H. Tawfick, R. H. Baughman, and A. J. Hart, *Science* **339**, 535 (2013)

17. A. J. Zhou, T. J. Zhu, X. B. Zhao, S. H. Yang, T. Dasgupta, C. Stiewe, R. Hassdorf, and E. Mueller, *J. Electron*. *Mater*. **39**, 2002 (2010)

18. E. Savary, F. Gascoin, and S. Marinel, *Dalton Trans.* **39**, 11074 (2010)

19. M. Ioannou, K. Chrissafis, E. Pavlidou, F. Gascoin, and T. Kyratsi, *J. Solid State Chem*. **197**, 172 (2013)

20. E. Savary, F. Gascoin, S. Marinel, and R. Heuguet, *Powder Technology* **228**, 295 (2012)

21. X. Chen, A. Weathers, S. Salta, L. Zhang, J. Zhou, J. B. Goodenough, and L. Shi, *J. Appl. Phys.* **114**, 173705 (2013)

22. I. Aoyama, M. I. Fedorov, V. K. Zaitsev, F. Y. Solomkin, I. S. Eremin, A. Y. Samunin, M. Mukoujima, S. Sano, and T. Tsuji, *Jpn*. *J*. *Appl*. *Phys*. **44**, 8562 (2005)

23. Unit cell determination via profile matching indicates a slight increase of the *a* parameter due to the insertion of Ge. Without germanium: a = 5.5226(1) Å, with germanium a = 5.5267(4) Å.

24. Q. R. Hou, W. Zhao, H. Y. Zhang, Y. B. Chen, and Y. J. He, *Phys*. *Stat*. *Sol*. *(a)* **203**, 2468 (2006)

Table Of Content entry :

Significant thermal diffusivity reduction in HMS / MWCNT composites made by ball milling and spark plasma sintering